



Abstract

Larger calving events in the Antarctic Ice Shelf (AIS) have been seen in the past few decades, and are an important ecological marker for the overall health of the ice shelves. We have used a novel Gaussian Random Field (GRF)-represented **data cube** in combination with **Attention U-Nets** to explore the predictability of calving events in the AIS. The data cube consists of several Essential Climate Variables (ECVs), which were selected based on their significance to the AIS, along with some supplementary data sources. Labelled calving events were collected from the 15 year inventory of Qi et al. [7], which required slight geospatial corrections before being rasterised. Trained U-Nets were subsequently analysed with Explainable AI (XAI), using a variation Guided Back Propagation [8] to produce **input saliency maps**. The U-Net models reached an **F1-score ≥ 0.9** , segmenting areas of future calving events. Expert evaluation of the combined input, saliency-maps, and predictions found the models seem to correspond well with current physical models.

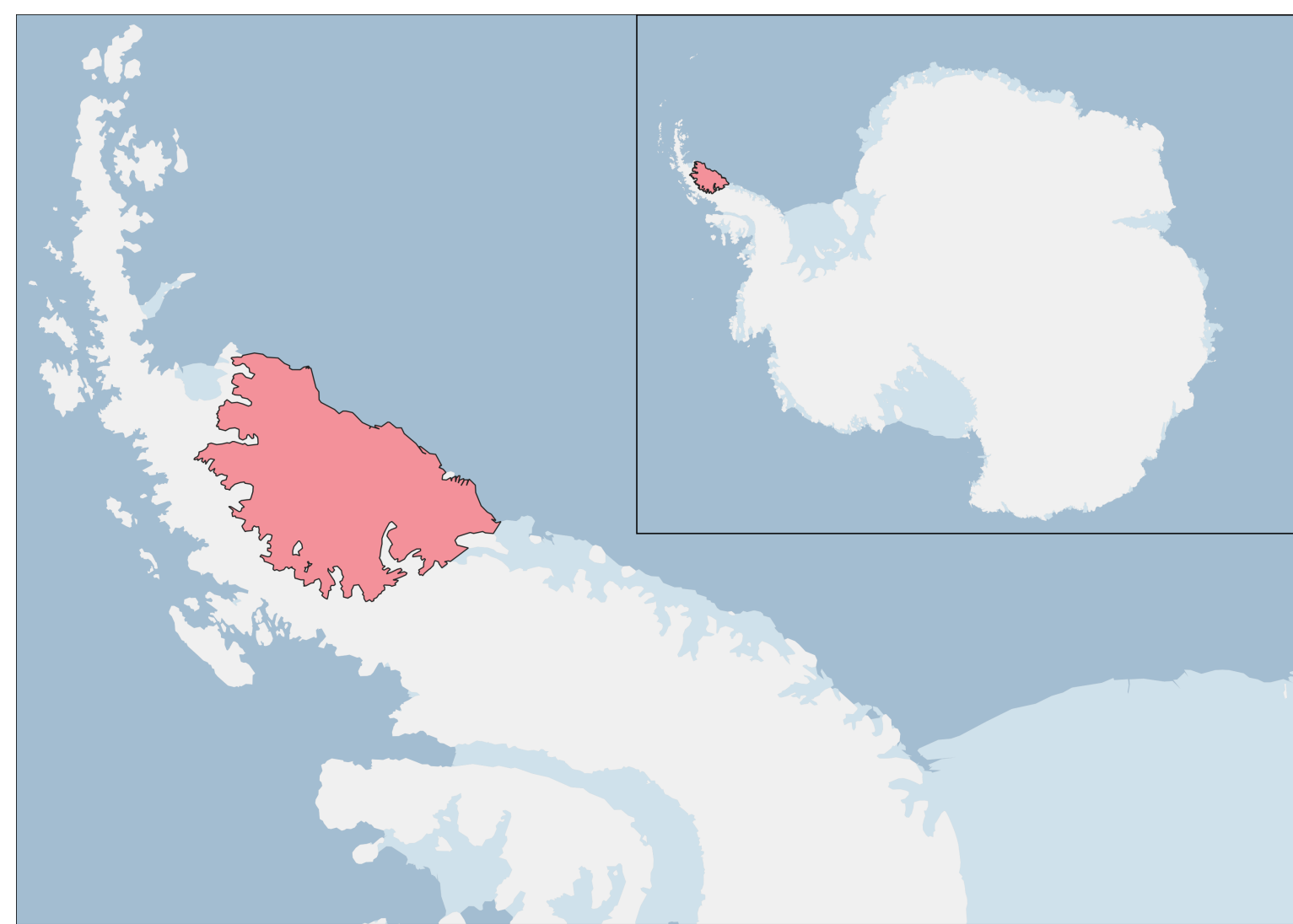


Figure 1: Location of first study site, Larsen C.

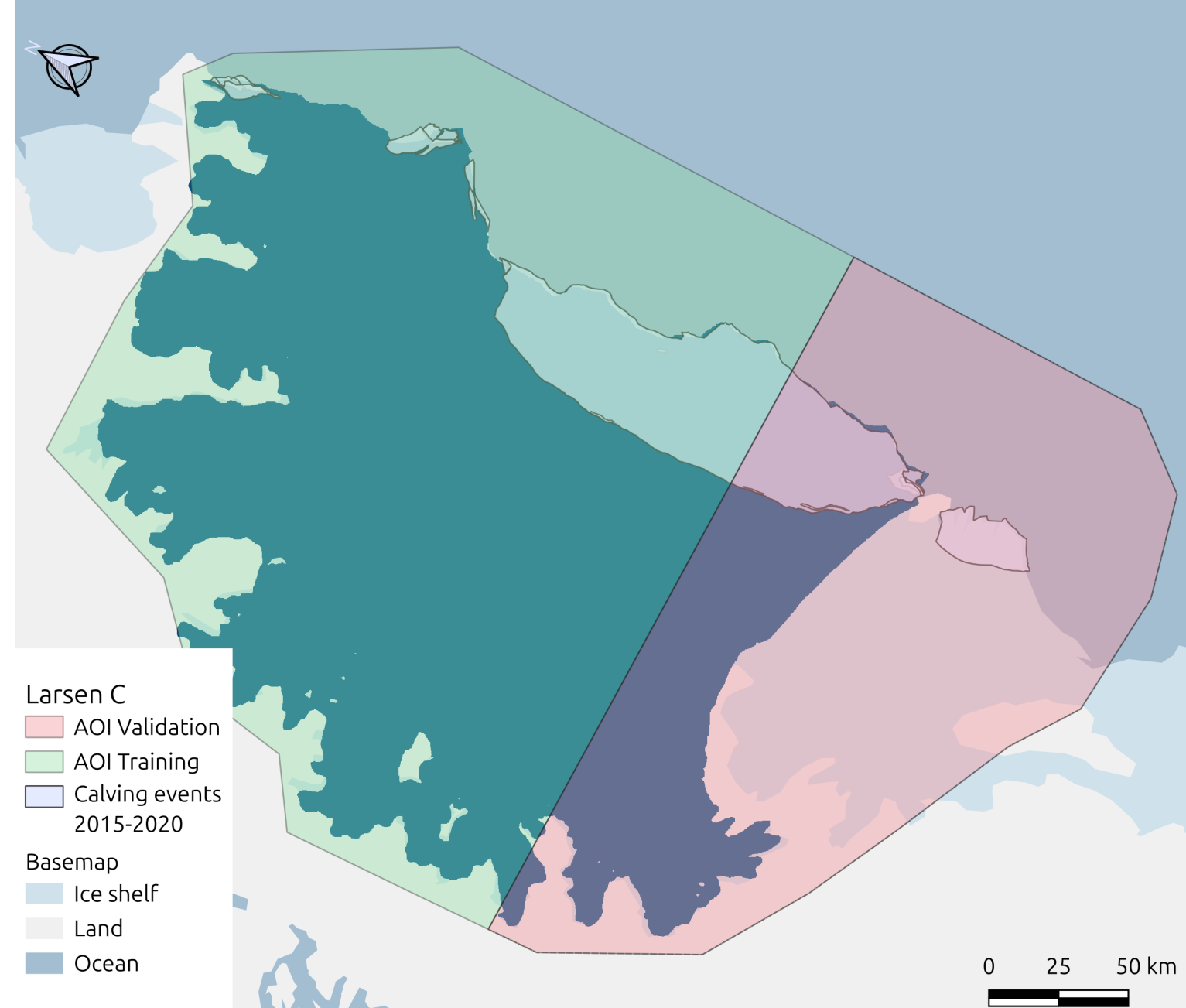


Figure 2: Data split, showing data coverage (dark blue). Calving events between 2015-2020 in light blue, with the major event of A-68 being the largest.

Model Summary

Model	
Model	Attention U-Net [6]
Activation	ReLU
Encoder Blocks	5
Base channels	16
Output channels	2
Optimizer	
Algorithm	AdamW [5]
Learning Rate	0.001
β_1	0.9
β_2	0.9
Weight Decay	0.1
Loss	
Loss Function	Focal Loss [4]
γ	3
classes	(no-calving, calving)
class weights	[1, 2]
reduction	mean
Data Augmentation	
Input-shape	364 x 364
Rotation	$\theta \in [0, \pm 45^\circ]$
P(Horiz.flip)	0.5
P(Vert.flip)	0.5
Center Clip	256 x 256

Table 1: Summary of parameters and hyperparameters used for model and training.

Acknowledgements

The Artificial Intelligence for Ice Shelves (AI4IS) project, of which this work constituted the first portion, was funded by the European Space Agency (ESA) as part of the AI4Science ITT (ESA Contract No 4000143299/23/I-DT)

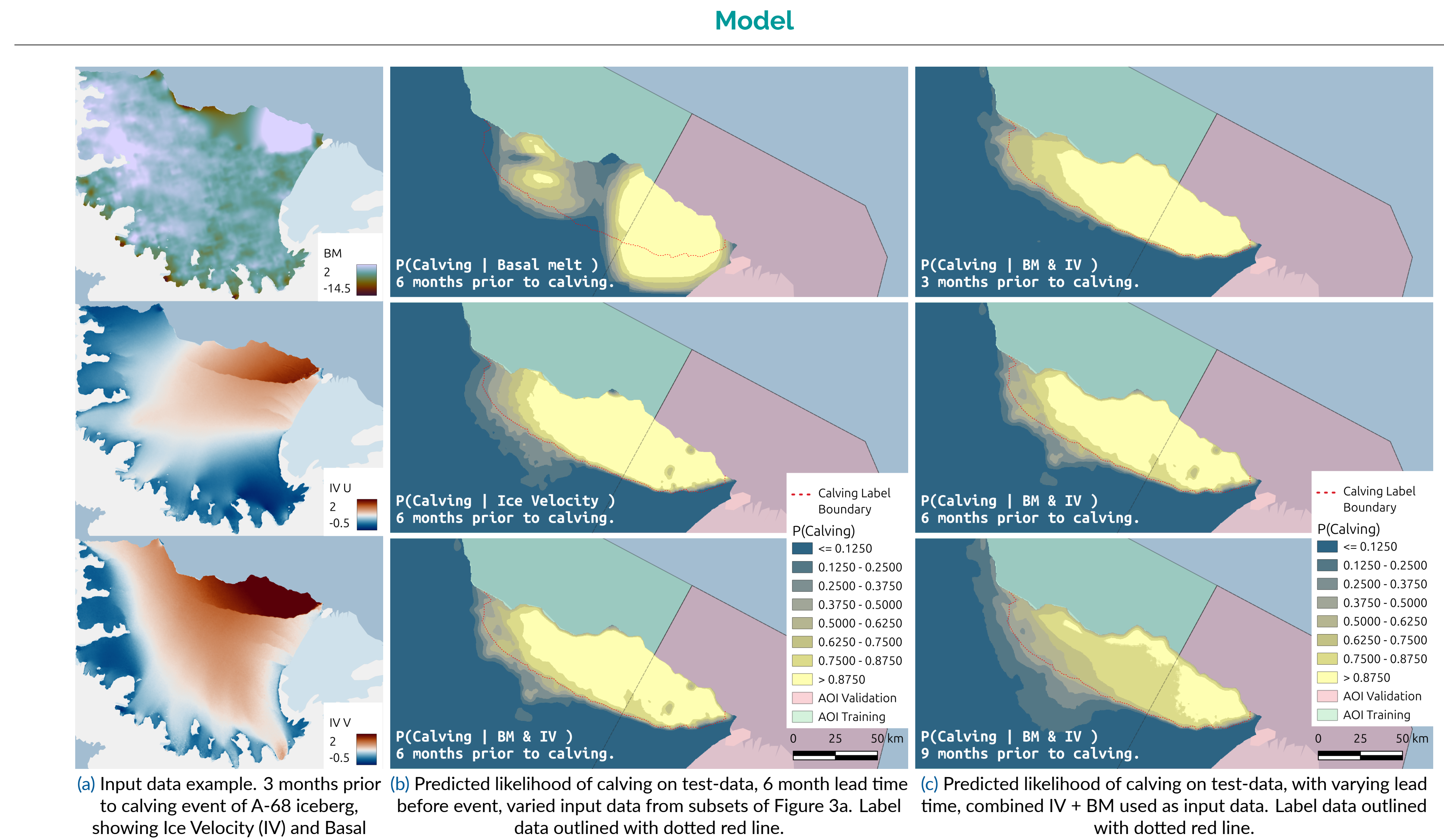


Figure 3: Example inputs from 3 month prior to the A-68 calving event are shown in Figure 3a. Figures 3b and 3c show outputs from models trained on subsets of the input example, and with modifications on lead-time respectively.

Dataset (source)	Original Resolution
IV [3]	200 x 200 m
Surface Mass Balance (SMB) [9]	27 x 27 km
Firm thickness [10]	27 x 27 km
Firm air content [10]	27 x 27 km
BM [2]	1000 x 1000 m
Wind Speed and direction (WS) [1]	31 x 31 km

Table 2: Table of datasets contained in the used version of Data Cube. All data was resampled from original resolution to 200 m resolution.

Temporal data splits

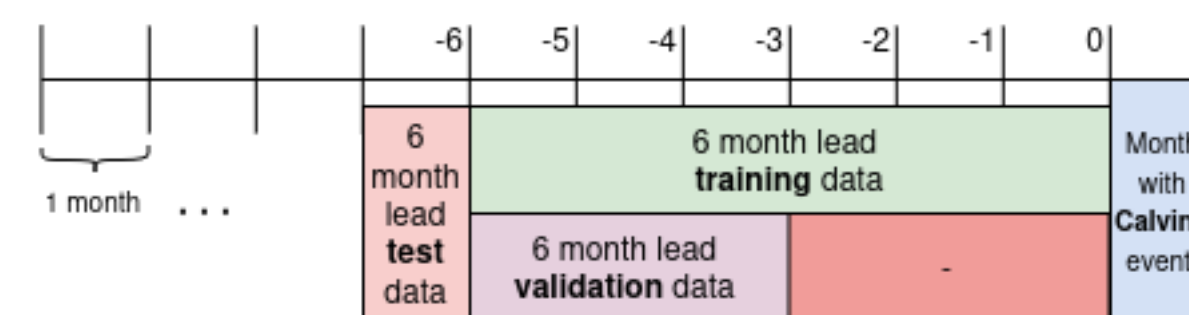


Figure 4: Example of 6 month temporal data split schema, showing the 3 month sampling window for validation, and the inclusion of lifting strategy.

Figure 4 showing the schema used for temporal split of data, where the "lead time" scheme intended to provide additional lifting by including temporally closer data as part of the training data. These splits were used in concert with the spatial split AOIs (Figure 2) for a combined spatiotemporal splitting strategy. The test-data was kept separate temporally and used for a qualitative evaluation by domain experts along with saliency-maps.

Raster-data samples from the data cube were given as inputs (Figure 3a), from which the models produce segmented maps with likelihood of belonging to a calving region (Figures 3b and 3c). The target shapes were derived from Qi et al. [7] (dotted red lines of calving in Figures 3b and 3c, original vector data shown as light blue in Figure 2).

Results

Subset	Lead time			
	3 months	6 months	9 months	12 months
IV	0.951 ± 0.015	<i>0.936 ± 0.0043</i>	0.927 ± 0.0085	0.945 ± 0.0073
BM	0.865 ± 0.0097	0.822 ± 0.024	0.785 ± 0.04	0.794 ± 0.0086
IV + BM	<i>0.941 ± 0.0036</i>	0.937 ± 0.0025	<i>0.926 ± 0.0019</i>	<i>0.928 ± 0.0032</i>
SMB	0.605 ± 0.11	0.622 ± 0.18	0.488 ± 0.0065	0.506 ± 0.011
WS	0.786 ± 0.02	0.739 ± 0.02	0.749 ± 0.009	0.778 ± 0.01
firm thickness	0.550 ± 0.1	0.596 ± 0.14	0.623 ± 0.14	0.630 ± 0.01
firm air content	0.491 ± 0.005	0.486 ± 0.009	0.487 ± 0.006	0.487 ± 0.0005

Table 3: Highest validation F1-score mean vs lead time. Highest F1-scores per lead time highlighted in bold, and second highest performance italicised. Values reported are the Mean (M) of highest F1-scores and their respective Standard Deviation (SD).

Table 3 shows how our models performed best when IV was part of the training data. The second strongest correlation to performance was BM, leading us to experiments with combined datasets of both IV and BM. These experiments resulted in a slightly reduced variance, but overall seemed to perform on par with the IV, with minor qualitative differences.

Explainability and Qualitative Evaluation

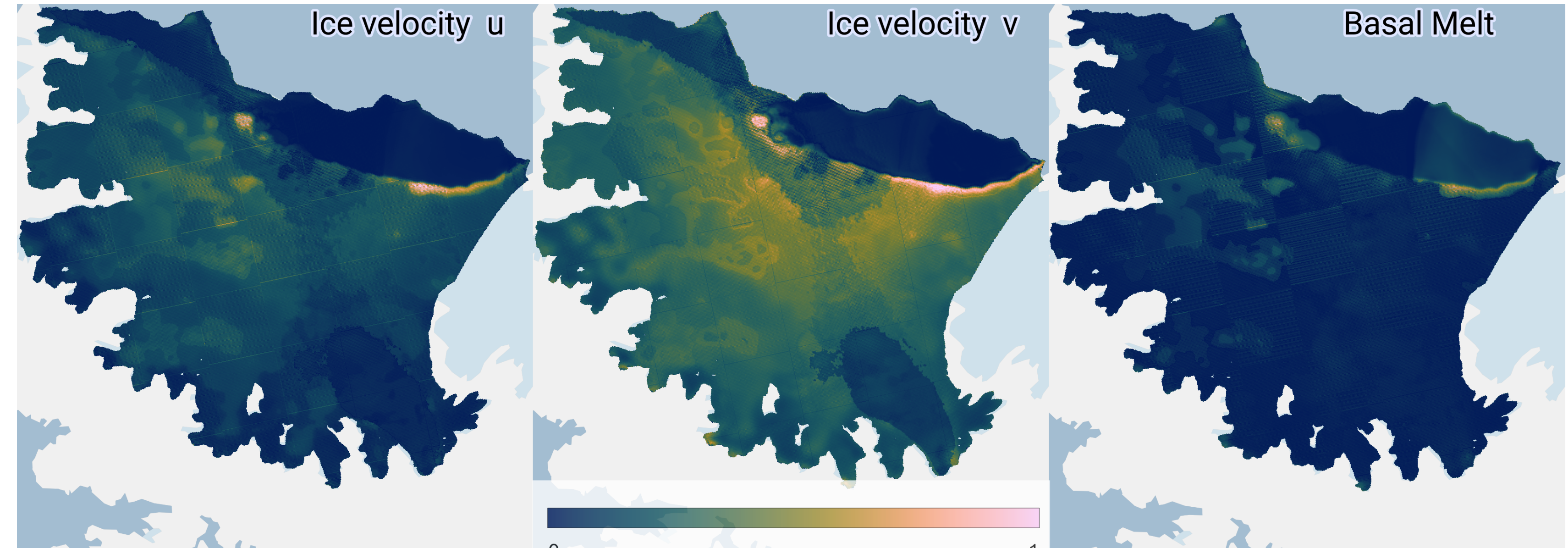


Figure 5: Model input-saliency across 3 input dimensions, as highlighted using Guided Back Propagation.

The trained models were analysed using a version of Guided Back Propagation [8] which made a saliency-map over the input variables. Normalised absolute values of saliences for positive calving classification are shown in Figure 5. The saliency maps, along with the model predictions and inputs, was presented for evaluation by domain experts from the Lancaster Environment Centre. Based on their evaluation the models seemed to align well with current models, and our current understanding of the dynamics of the ice shelves.

References

- [1] Copernicus Climate Change Service. ERA5 Monthly Averaged Data on Single Levels from 1940 to Present. 2019. DOI: 10.24381/CDS.F17050D7.
- [2] Benjamin Davison. *Data and Code for: 'Annual Mass Budget of Antarctic Ice Shelves from 1997 to 2021'*. June 2023. DOI: 10.5281/ZENODO.8052518.
- [3] ENVEO et al. *ESA Antarctic Ice Sheet Climate Change Initiative (Antarctic_Ice_Sheet_cci): Antarctic Ice Sheet Monthly Velocity from 2017 to 2020*. Derived from Sentinel-1, V1. 2021. DOI: 10.5285/00FE09EFC58446E8980992A617F632F.
- [4] Tsung-Yi Lin et al. 'Focal Loss for Dense Object Detection'. In: *Proceedings of the IEEE international conference on computer vision* 1 (2017), pp. 2980-2988. DOI: 10.1109/TPAMI.2018.2858826.
- [5] Ilya Loshchilov and Frank Hutter. 'Decoupled Weight Decay Regularization'. Jan. 2019. DOI: 10.48550/arXiv.1711.05101. arXiv: 1711.05101 [cs].
- [6] Ostan Oktay et al. 'Attention U-Net: Learning Where to Look for the Pancreas'. May 2018. DOI: 10.48550/arXiv.1804.03999. arXiv: 1804.03999 [cs].
- [7] M. Qi et al. 'A 15-Year Circum-Antarctic Iceberg Calving Dataset Derived from Continuous Satellite Observations'. In: *Earth System Science Data* 13 (2021), pp. 4583-4601. DOI: 10.5194/esd-13-4583-2021.
- [8] Jost Tobias Springenberg et al. 'Striving for Simplicity: The All Convolutional Net'. Apr. 2015. DOI: 10.48550/arXiv.1412.6806. arXiv: 1412.6806 [cs].
- [9] Christiaan T. Van Dalem et al. 'First Results of the Polar Regional Climate Model RACMO2.4'. In: *The Cryosphere* 18 (Sept. 2024), pp. 4065-4088. ISSN: 1994-0424. DOI: 10.5194/tc-18-4065-2024.
- [10] Sanne B. M. Veldhuisen et al. 'Characteristics of the 1979-2020 Antarctic Firn Layer Simulated with IMAU-FDM v1.2'. In: *The Cryosphere* 17 (Apr. 2023), pp. 1675-1696. ISSN: 1994-0424. DOI: 10.5194/tc-17-1675-2023.